Draft version December 12, 2018
Typeset using LaTeX default style in AASTeX62

Testing Gravity using Type Ia Supernovae Discovered by LSST

A. G. Kim,[1] S. BenZvi,[2] C. Harper,[1] C. Ju,[1] D. Huterer,[3] and others

[1] *Physics Division, Lawrence Berkeley National Laboratory, 1 Cyclotron Road, Berkeley, CA, 94720*
[2] *Department of Physics and Astronomy, University of Rochester, Rochester, NY 14627, USA*
[3] *Department of Physics, University of Michigan, 450 Church Street, Ann Arbor, MI 48109, USA*

ABSTRACT

ZTF today and LSST in the upcoming decade will increase the number of identified $z < 0.2$ Type Ia supernovae (SNe Ia) from the hundreds to the hundreds of thousands. The increase in the number density of SNe Ia, in parallel with improvements in the standardization of their absolute magnitudes, now make them competitive probes of the growth of structure. The peculiar velocity power spectrum derived from SNe Ia is sensitive to the product of the linear growth and amplitude of structure $f\sigma_8$. Cross-correlation with synergistic galaxy surveys further constrains $f\sigma_8$ and the galaxy bias. Velocities SNe Ia in the next decade will measure the growth of structure a powerful test of General Relativity in the local $z < 0.2$ Universe.

1. CONNECTION BETWEEN TYPE IA SUPERNOVAE CORRELATIONS AND GRAVITY

The growth of structure depends on the expansion history of the Universe, the nature and density of its contents, and gravity. It is therefore a powerful probe of cosmology and dark energy. Growth of structure can be measured from the baryonic structures in the Universe and from the peculiar velocities of test masses therein. Peculiar velocities are the motions, on top of the cosmological expansion, caused by the gravitational attraction and repulsion due to inhomogeneities in the Universe. The peculiar velocity of an object wth a given absolute magnitude is determined from its observer magnitude and redshift. Given a background cosmology, the observed magnitude provides an estimate of the cosmological redshift. Peculiar velocity accounts for the difference between the cosmological and observer redshift.

Baryonic structures and peculiar velocities provide a measurement of the combination fD. D is the "linear growth factor" that gives the overall amplitude of overdensities and the "linear growth rate"

$$f \equiv \frac{d\ln D}{d\ln a}$$

is how that amplitude changes with redshift. General Relativity predicts $f \approx \Omega_M^\gamma$ (with D determined accordingly) when $\gamma = 0.55$, whereas other gravity models can be similarly described with different values of γ (Linder & Cahn 2007). Thus growth of structure, through the measurement of fD, provides a test of General Relativity and breaks degeneracies between gravitational and dark energy models that explain the accelerating expansion of the Universe. The parameter σ_8, the standard deviation of overdensities in $8h^{-1}$Mpc spheres, is commonly used to normalize the overall amplitude of overdensities instead of D, and so the standard parameterization used by the community is $f\sigma_8$.

Baryonic structures are sensitive to $f\sigma_8$ through redshift space distortions (RSD), which gives the combination $(b + f\mu^2)\sigma_8$ where b is the bias between the tracer and dark matter and μ gives the angular separation. Correlations between peculiar velocities are sensitive to $f\sigma_8(H_0 d_L)^{-1}$. They are independent of the tracer bias because all sources of mass, predominantly dark matter, contribute to the dynamics. As mentioned earlier, peculiar velocities are measured relative to the background cosmological expansion that leads to the dependence on $H_0 d_L$. The cross-correlation between structure and peculiar velocity within the same volume come from the same overdensities and hence provide independent information unsusceptible to sample variance (Gordon et al. 2007).

Tracers with precisely known absolute magnitude provide precise cosmological redshifts and hence peculiar velocities. The current generation of peculiar velocity studies use $10^3 - 10^5$ galaxies with Fundamental Plane and Tully-Fisher distances (Masters et al. 2008; Springob et al. 2014; Tully et al. 2016). Next generation surveys WALLABY (Johnston et al. 2008) and TAIPAN (da Cunha et al. 2017) are designed to increase these sample size by an order of magnitude. The galaxies have absolute magnitude uncertainties of ~ 0.4 mag.

The current sample of SNe Ia has a low number density compared to Fundamental Plane and Tully-Fisher galaxies. Nevertheless, their low intrinsic-magnitude uncertainties can can provide peculiar velocities (expressed equivalently

Redshift	RSD	RSD + PV	cumulative
$0.00 < z < 0.05$	66.3	13.9	13.9
$0.05 < z < 0.10$	24.6	7.3	6.5
$0.10 < z < 0.15$	14.8	5.8	4.3
$0.15 < z < 0.20$	10.6	5.0	3.3
$0.20 < z < 0.25$	8.3	4.4	2.6
$0.25 < z < 0.30$	6.8	4.0	2.2

Table 1. Projected percent uncertainties in $f\sigma_8$ from a 10-year LSST SN survey with 5% distance uncertainties from Howlett et al. (2017a). RSD is from clustering, and RSD + PV is from joint clustering and peculiar velocities. The cumulative column shows the effective uncertainty from combining the redshift and all other shallower redshift bins.

as peculiar magnitudes) of their host galaxies (Hui & Greene 2006; Davis et al. 2011). Existing SN Ia samples have been used to test and ultimately find spatial correlations in peculiar velocities that may be attributed to the growth of structure Abate & Lahav (2008); Huterer et al. (2015, 2017). However, the ston is currently insufficient to perform a meaningful test of GR.

Two advances in the upcoming decade will make SNe Ia important probes of $f\sigma_8$. First, the precision of SN Ia distances can be improved. The commonly-used empirical 2-parameter SED model yields $\sigma_M \gtrsim 0.12$ mag absolute magnitude dispersion. However, SNe transmit more information than just the light curve shape and single color used in current analysis. Recent studies indicate that with the right data, SNe absolute magnitudes can be calibrated to $\sigma_M \lesssim 0.08$ mag (see e.g. Barone-Nugent et al. 2012; Fakhouri et al. 2015). One such SN is worth $\gtrsim 25$ galaxies with 0.4 mag absolute magnitude uncertainty. Secondly, ZTF today and LSST in the upcoming decade will increase the number of identified $z < 0.3$ Type Ia supernovae (SNe Ia) from the hundreds to the hundreds of thousands. This is a sample size comparable to those projected by WALLABY and TAIPAN.

The precision in $f\sigma_8$ derived from the baseline WFD ten-year SN Ia discoveries has been projected by Howlett et al. (2017a), from both their RSD and peculiar velocities. The results are summarized in Table 1, where a 5% distance uncertainty is assumed for each supernova. SNe Ia alone can provide a 2% measurement of $f\sigma_8$ at $z < 0.3$ redshifts lower than where galaxy, cluster, and Lyα RSD measurements are sensitive. A joint galaxy RSD and SN peculiar velocity will be even more powerful. **Add a SN PV + DESI-like BGS column and/or a PV-only column with Cullan's code?**

The projected precisions for LSST-discovered SNe Ia have a number of interesting features. Relative to RSD, particular velocities contribute increasingly $f\sigma_8$ precision with decreasing redshift. At redshift 0.3 the differential gain from adding peculiar velocities to the RSD measurement is small. Despite the significant gain in volume and numbers of supernovae, the $f\sigma_8$ uncertainty in increasing redshift bins asymptotes such that the differential gain in the cumulative uncertainty is small for surveys with increasing maximum redshift. For $z > 0.1$, the volume is sufficiently large that we are not yet sample variance limited given the LSST sample.

2. IMPORTANT ELEMENTS IN DESIGNING A SUPERNOVA SURVEY TO MEASURE $f\sigma_8$

Howlett et al. (2017a) perform their analysis in Fourier space, where the Fisher information matrix of a random Gaussian field with mean zero and covariance $C(k)$ parameterized by λ is approximated by

$$F_{ij} = \frac{V}{2} \int \frac{d^3k}{(2\pi)^3} \mathrm{Tr}\left[C^{-1}\frac{\partial C}{\partial \lambda_i} C^{-1} \frac{\partial C}{\partial \lambda_j}\right], \tag{1}$$

where the covariance for the velocity-velocity correlation

$$C = P_{vv}(k) + \frac{\sigma^2}{n} \tag{2}$$

is dependent on the power spectrum, noise in the velocity measurement, and the density of velocity probes (Howlett et al. 2017b).

The survey parameters that determine parameter precision are the volume V, which in turn can be parameterized by the survey solid angle Ω and the redshift depth z_{max} ; the number density of sources n; and the intrinsic magnitude dispersion σ_M, where magnitude and velocity dispersions are related by $\sigma_M = \frac{5}{\ln 10}\frac{1+z}{z}\sigma$. For surveys of fixed depth,

the variance of $f\sigma_8$ in the sample-variance limit is inversely proportional to the survey solid-angle Ω, whereas in the shot-noise limit the variance is inversely proportional to $\Omega n^2 \propto N^2/\Omega$, where n is the number density, and N is the total number of supernovae.

LSST is expected to discover all $z < 0.3$ SNe Ia before maximum light in its active Wide Fast Deep (WFD) survey area. The nominal observing strategy will obtain photometry every couple of days rotating through the 6 *grizy* bands.

The quality of supernova follow-up is an important factor in how well a peculiar-velocity survey can measure $f\sigma_8$. LSST SM Ia light curves from the WFD survey, with their relatively poor sampling, plus a spectroscopic redshift can give $\sigma_M \sim 0.15$ mag. Non-LSST follow-up including infrared data (Barone-Nugent et al. 2012) or spectrophotometry at peak brightness (Fakhouri et al. 2015) are projected to give $\sigma_M \lesssim 0.08$ mag. Uncertainties in $f\sigma_8$ depend on σ_M^2/n so the improvement between 0.08 and 0.15 mag dispersions is equivalent to a factor of 3.52 in number density, or in survey duration given the expected saturation of $z < 0.3$ SN Ia discoveries.

The variance in $f\sigma_8$ is proportional to solid angle Ω given a fixed redshift depth and σ_M^2/n. The baseline LSST survey covers 18,000 sq. deg, at $-75 \lesssim \delta \lesssim 15$ avoiding the Galactic plane. Larger solid-angle coverage for $z < -0.3$ SN Ia searches, beyond the LSST baseline, benefits peculiar-velocity science. Complementary northern-hemisphere surveys and LSST-expanded or independent coverage of the southern pole, could double the sky coverage and halve the variance in $f\sigma_8$.

LSST can be taken to be a SN Ia discovery plus light-curve builder, or a discovery machine only. The former comes with a simplified follow-up program of typing and/or redshift collection but with higher intrinsic magnitude dispersion. The latter requires additional follow-up resources to gather more information per supernova to lower the intrinsic magnitude dispersion.

ZTF and Future-ZTF. Access close to 4π. LSST does not survey the southern equatorial pole.

APPENDIX

A. REANALYSIS IN CONFIGURATION SPACE

This Appendix describes a new analysis used to project precisions on $f\sigma_8$ using peculiar velocities derived from SNe Ia. This analysis may or may not be useful for the Decadal Survey White Paper, but will be helpful for LSST planning. While there have been a number of articles on the subject, our analysis brings a higher level of fidelity than sought previously. We simulate SNe Ia hosted by galaxies in a mock galaxy catalog. The numbers of SNe are sufficiently small to allow fast evaluations of the likelihood, which enable the determination of parameter posteriors using MCMC on reasonable computing timescales. We can use our machinery to compare different survey parameters, such as redshift depth, total numbers of supernovae, non-uniform spatial density, solid angle/survey geometry, and SN Ia intrinsic magnitude dispersion. Adding the cross-correlation between galaxy-count and peculiar-velocity surveys is active work, so we can quantify the suppression of sample variance achieved when considering matter-densities and velocities within the same volume (Gordon et al. 2007).

B. SIMULATED DATA

The cosmoDC2 (v1.0) covering 706 sq. deg is used[1]. The catalog is based on a Flat ΛCDM model with $H_0 = 71$ km s^{-1}, $\Omega_M = 0.265$, $\Omega_B = 0.0448$, and $\Omega_\nu = 0$. Each galaxy has its cosmological redshift, the x-, y-, z-components of its peculiar velocity from which the radial peculiar velocity is determined, and its star formation rate and stellar mass from which the supernova rate of each host is determined using Smith et al. (2012). This host-based rate underestimates the expected discovery based on the volumetric rate of Dilday et al. (2010). The volumetric rate is more robust, so we boost the SN production by a factor 2.4 to get the 10-year volumetric rate expectation. The total number of simulated SNe is greater than the total number of possibly useful supernova discoveries, since most fields cannot be continuously monitored throughout the year from most ground-based observatories.

Each supernova is assigned a magnitude based on the distance modulus of its cosmological redshift plus a random term drawn from a Normal distribution σ_M, which for simplicity is the same for all supernovae and captures both intrinsic magnitude dispersion and measurement uncertainty. No other corrections are applied to the observed magnitude. Dipole effects of the heliocentric motion with respect to the CMB and of the galaxies with respect to the CMB are

[1] We previously used Buzzard (v1.6) galaxy catalog is used, but it was found to give peculiar velocities inconsistent with general relativity. As we will see, cosmoDC2 (v1.0) is consistent with GR.

ignored: referring to Davis et al. (2011), the effects in Eq. 18 are not included. Including these effects are straightforward but is computationally expensive and does not affect our conclusions.

We consider a maximum redshift of $z = 0.2$ because over ten years the noise is not sample-variance dominated, meaning that the differential improvement in the precision of $f\sigma_8$ due to a lower-redshift supernova is greater than that due to a high-redshift supernova. Following all LSST SNe Ia below this redshift would likely saturate available follow-up resources.

C. ANALYSIS

The analysis is almost identical to that of Huterer et al. (2015, 2017), except as noted later. The peculiar magnitude is given by

$$\delta_m = (m - M) - \mu(z; H_0, \Omega_M, \Omega_\Lambda). \tag{C1}$$

We introduce one free parameter $\mathcal{M} = M - 5\log H_0 + \text{const}$ and do not consider the other cosmological parameters, whose effects are relatively weak at low-redshift.

The peculiar magnitude correlation function $\xi_{\delta m \delta m}$ (Davis et al. 2011; Huterer et al. 2015) expected from General Relativity acting on the CMB matter density power spectrum is calculated using CAMB (Lewis & Bridle 2002) assuming the same cosmological parameters used for the cosmoDC2 catalog. Our model for the data covariance is

$$C_{ij} = A\xi_{\delta m \delta m}(\mathbf{r_i}, \mathbf{r_j}) + \frac{\sigma_M^2}{N_i}\delta_{ij} + \sigma_{NL}^2(z_i; \sigma_v)\delta_{ij}, \tag{C2}$$

where N_i is the number of SNe Ia in galaxy i and σ_M is the intrinsic SN magnitude dispersion. The model is used to test General Relativity through deviations from $A = 1$ but is not sensitive to deviations from the linearized GR expectation of the shape of the power spectrum ξ. Nevertheless, for convenience we say that our model gives $f\sigma_8 = A(f\sigma_8)^{GR}$, where $(f\sigma_8)^{GR}$ is the expectation from General Relativity. The final term includes extra magnitude dispersion produced by non-linear effects on velocity, parameterized with σ_v, such that

$$\sigma_{NL} = \frac{5}{\ln 10}\frac{1+\bar{z}}{\bar{z}}\sigma_v, \tag{C3}$$

where $\bar{z}$ is the cosmological redshift of the host galaxy. We note that the CAMB calculation of ξ includes non-linear corrections, which actually may be a bad thing for peculiar velocities (Hahn et al. 2015). Such subtleties are unimportant as Huterer et al. (2015) find that their results are insensitive to whether non-linear corrections are or are not included.

For all analyses we remove supernovae below observed $z_{min} = 0.01$ in order to reduce errors made in the first-order transformation between velocity and magnitude. This cut removes a small volume relative to the full survey.

The posterior of the parameters is sampled using emcee. The likelihood is the Normal distribution with the data in Eq. C1 and covariance matrix in Eq. C2. The priors are positive and flat for A, flat for M, positive Cauchy(0.08, 0.5) for σ_M, and positive Cauchy(0, 600 km s^{-1}) for σ_v.

Direct tests of non-GR models for which Poisson's equation or the linear approximation does not apply requires a model-dependent ξ. We defer the analysis of such higher-fidelity models to later work.

D. RESULTS OF SUBSETS

The ston in $f\sigma_8$ is calculated for different subsamples of the simulated data. For each subsample the mean and standard deviation, $(\bar{A}, \sigma_A)$ of the amplitude parameter is determined. The ston in $f\sigma_8$ for the subsample is thus $\bar{A}\sigma_A^{-1}$, and that for a 18,000 sq. deg. survey is approximated by $\sqrt{18000/760}\bar{A}\sigma_A^{-1}$. The effective constraining power of a single supernova in the subset is chracterized by $\bar{A}\sigma_A^{-1}N_{gal}^{-0.5}$.

Different parameters describing the input simulated data define the subsamples, which are used to explore the range of possible survey strategies. The varied parameters are the redshift range, z_{max}, intrinsic magnitude dispersion, σ_M, and SN number density, $n = \phi n_{10}$, where n_{10} is the 10-year total number density. In general a given point of sky is not monitored over the full year. The fit posterior for one representative subsample, with input $z_{max} = 0.2$, $\sigma_M = 0.08$, $\phi = 0.65$, is shown in Figure 1. For all subsamples, there is no evidence for non-convergence of the MCMC chains. The parameter σ_v, not included in Huterer et al. (2015, 2017), is found to be consistent with zero, poorly constrained, and very weakly correlated with A. Table 2 gives the results for the different subsamples.

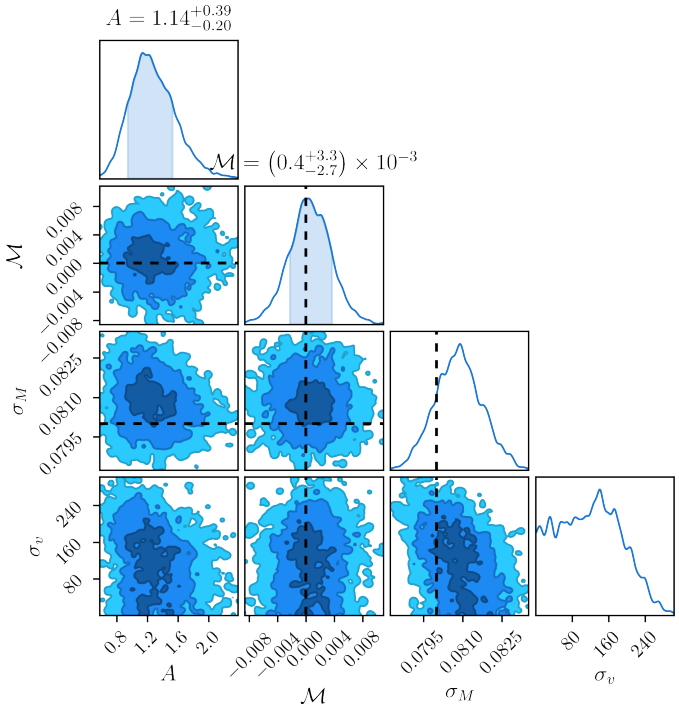

Figure 1. Confidence regions for the model parameters. $A = (f\sigma_8)/(f\sigma_8)_{GR}$, $\mathcal{M}$ is the supernova absolute magnitude, σ_M is the magnitude dispersion, and σ_v is the non-linear contribution to peculiar velocity. This result is for the subset $z_{max} = 0.2$, $\sigma_M = 0.08$, $\phi = 0.65$. The dotted lines represent the inputs of the supernova part of the simulation.

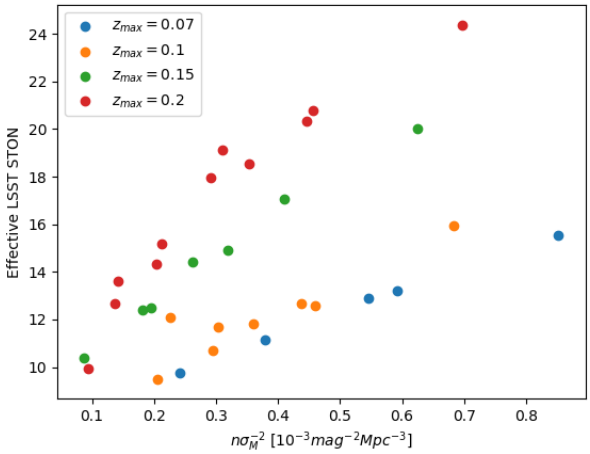

Figure 2. Effective LSST ston as a function of input $n\sigma_M^{-2}$. The points are color-coded for different z_{max}.

In Fourier space, the data covariance is a combination of sample and shot noise (Eq. 2). In Figure 2 the effective LSST ston is plotted as a function of input $n\sigma_M^{-2}$ for different z_{max}. For all cases, the ston improves with larger $n\sigma_M^{-2}$ showing that the sample-variance limit has not been reached, though the shallowing of the slopes for shallower surveys shows that it does contribute non-negligibly. The fact that the ston is not constant indicates that not of the subsamples is sample-variance limited, though its non-linearity indicates that it is non-negligible.

A SN peculiar survey benefits from greater redshift depth z_{max} due to the increase in volume and numbers of supernovae. However, for fixed magnitude uncertainty peculiar-velocity uncertainties increase with redshift and the follow-up of fainter distant SNe requires more resources. Table 2 shows that the effective worth of each supernova

z_{max}	ϕ	σ_M	N_{gal}	$\bar{A}$	σ_A	$\bar{A}\sigma_A^{-1}N_{gal}^{0.5}$	$\bar{A}\sigma_A^{-1}(18000/760)^{0.5}$
0.07	0.65	0.08	392	1.34	0.49	0.137	13.21
0.07	1.00	0.08	563	1.16	0.36	0.135	15.55
0.07	1.00	0.10	563	1.27	0.48	0.112	12.88
0.07	1.00	0.12	563	1.41	0.61	0.097	11.15
0.07	1.00	0.15	563	1.64	0.82	0.084	9.74
0.10	0.30	0.08	429	1.26	0.51	0.120	12.09
0.10	0.50	0.08	683	1.02	0.42	0.093	11.84
0.10	0.65	0.08	873	0.89	0.35	0.087	12.57
0.10	0.65	0.10	873	1.01	0.46	0.075	10.72
0.10	0.65	0.12	873	1.11	0.57	0.066	9.48
0.10	1.00	0.08	1294	0.91	0.28	0.091	15.96
0.10	1.00	0.10	1294	0.95	0.36	0.072	12.66
0.10	1.00	0.12	1294	1.04	0.43	0.067	11.71
0.15	0.30	0.08	1215	1.42	0.55	0.074	12.48
0.15	0.30	0.12	1215	1.97	0.92	0.061	10.36
0.15	0.50	0.08	1982	1.12	0.37	0.069	14.93
0.15	0.65	0.08	2541	1.15	0.33	0.070	17.05
0.15	0.65	0.10	2541	1.15	0.39	0.059	14.43
0.15	0.65	0.12	2541	1.30	0.51	0.051	12.42
0.15	1.00	0.08	3870	1.00	0.24	0.066	20.00
0.20	0.20	0.08	2021	1.66	0.59	0.062	13.61
0.20	0.30	0.08	3023	1.34	0.43	0.057	15.16
0.20	0.30	0.10	3023	1.40	0.54	0.047	12.68
0.20	0.30	0.12	3023	1.48	0.72	0.037	9.95
0.20	0.50	0.08	5015	1.13	0.30	0.054	18.54
0.20	0.65	0.08	6491	1.28	0.30	0.053	20.79
0.20	0.65	0.10	6491	1.24	0.34	0.046	17.95
0.20	0.65	0.12	6491	1.33	0.45	0.037	14.33
0.20	1.00	0.08	9901	1.18	0.23	0.050	24.38
0.20	1.00	0.10	9901	1.06	0.25	0.042	20.33
0.20	1.00	0.12	9901	1.09	0.28	0.040	19.13

Table 2. ston in A or equivalently $f\sigma_8$ for surveys parameterized by the maximum redshift z_{max}, the fraction of total supernovae in 10 years "fraction", intrinsic magnitude dispersion σ_{SN}. The number of galaxies N_{gal}, the signal $\bar{A}$ and its uncertainty σ_A are for the cosmoDC2 (v1.0) 760 sq. deg. volume only. The uncertainty "per" supernova is given by $\sigma_A N_{gal}^{-0.5}$. The ston, scaled to an LSST solid angle, is given as $\bar{A}\sigma_A^{-1}(18000/760)^{0.5}$.

($\sigma_A N_{gal}^{-0.5}$) diminishes with increasing survey depth. The table also shows that for $\sigma_M = 0.08$ mag, the subsample with $z_{max} = 0.1$ with 1294 supernovae yields a ston of 15.96, whereas a sample with $z_{max} = 0.2$ with 2021 supernovae has a lower ston of 13.61. Within the range of surveys considered, a lower-redshift supernova is more valuable than one at high redshift. For both scientific and resource reasons, it is best to devote resources to the lowest possible redshifts.

$\phi \sim 0.65$ is an effective number density of discovered supernovae with light-curve coverage observed in 10 years

REFERENCES

Abate, A., & Lahav, O. 2008, MNRAS, 389, L47, doi: 10.1111/j.1745-3933.2008.00519.x

Barone-Nugent, R. L., Lidman, C., Wyithe, J. S. B., et al. 2012, MNRAS, 425, 1007, doi: 10.1111/j.1365-2966.2012.21412.x

da Cunha, E., Hopkins, A. M., Colless, M., et al. 2017, Publications of the Astronomical Society of Australia, 34, e047, doi: 10.1017/pasa.2017.41

Davis, T. M., Hui, L., Frieman, J. A., et al. 2011, ApJ, 741, 67, doi: 10.1088/0004-637X/741/1/67

Dilday, B., Smith, M., Bassett, B., et al. 2010, ApJ, 713, 1026, doi: 10.1088/0004-637X/713/2/1026

Fakhouri, H. K., Boone, K., Aldering, G., et al. 2015, ApJ, 815, 58, doi: 10.1088/0004-637X/815/1/58

Gordon, C., Land, K., & Slosar, A. 2007, PRL, 99, 081301, doi: 10.1103/PhysRevLett.99.081301

Hahn, O., Angulo, R. E., & Abel, T. 2015, MNRAS, 454, 3920, doi: 10.1093/mnras/stv2179

Howlett, C., Robotham, A. S. G., Lagos, C. D. P., & Kim, A. G. 2017a, ApJ, 847, 128, doi: 10.3847/1538-4357/aa88c8

Howlett, C., Staveley-Smith, L., & Blake, C. 2017b, MNRAS, 464, 2517, doi: 10.1093/mnras/stw2466

Hui, L., & Greene, P. B. 2006, PRD, 73, 123526, doi: 10.1103/PhysRevD.73.123526

Huterer, D., Shafer, D. L., & Schmidt, F. 2015, JCAP, 12, 033, doi: 10.1088/1475-7516/2015/12/033

Huterer, D., Shafer, D. L., Scolnic, D. M., & Schmidt, F. 2017, JCAP, 5, 015, doi: 10.1088/1475-7516/2017/05/015

Johnston, S., Taylor, R., Bailes, M., et al. 2008, Experimental Astronomy, 22, 151, doi: 10.1007/s10686-008-9124-7

Lewis, A., & Bridle, S. 2002, PhRvD, 66, 103511, doi: 10.1103/PhysRevD.66.103511

Linder, E. V., & Cahn, R. N. 2007, Astroparticle Physics, 28, 481, doi: 10.1016/j.astropartphys.2007.09.003

Masters, K. L., Springob, C. M., & Huchra, J. P. 2008, AJ, 135, 1738, doi: 10.1088/0004-6256/135/5/1738

Smith, M., Nichol, R. C., Dilday, B., et al. 2012, ApJ, 755, 61, doi: 10.1088/0004-637X/755/1/61

Springob, C. M., Magoulas, C., Colless, M., et al. 2014, MNRAS, 445, 2677, doi: 10.1093/mnras/stu1743

Tully, R. B., Courtois, H. M., & Sorce, J. G. 2016, AJ, 152, 50, doi: 10.3847/0004-6256/152/2/50